EUROPEAN JOURNAL OF PURE AND APPLIED MATHEMATICS
2025, Vol. 18, Issue 4, Article Number 6869
ISSN 1307-5543 – ejpam.com
Published by New York Business Global

Multi-Parametric Study of Convective Heat Transfer in a Magnetized Wavy Cavity Using Hybrid Nanofluids for Thermal Management Applications

Khamis Al Kalbani[1], Nidal Ratib Anakira[1], M. J. Uddin[2], Ali Fareed Al Jassar[1], Ala Amourah[1,3,*], Tala Sasa[4]

[1] *Mathematics Education Program, Faculty of Education and Arts, Sohar University, Sohar 311, Oman*
[2] *Department of Mathematical and Physical Sciences, University of Nizwa, Nizwa, Sultanate of Oman*
[3] *Jadara University Research Center, Jadara University, Jordan*
[4] *Department of Mathematics, Faculty of Science, Applied Science Private University, Amman, Jordan*

Abstract. This study presents a comprehensive numerical investigation of natural convective heat transfer in a wavy-walled enclosure filled with a hybrid nanofluid consisting of copper (Cu) and aluminum oxide (Al_2O_3) nanoparticles dispersed in a water-ethylene glycol (EG) base fluid. Natural convection in such enclosures is widely encountered in electronics cooling, energy devices, and magnetic field-controlled thermal systems, which motivates the present study. A range of water-EG mixture ratios ($95\%-5\%, 90\%-10\%, 80\%-20\%, 60\%-40\%, 50\%-50\%$), including the limiting cases of pure water and pure EG, is considered to evaluate the influence of base fluid composition on thermal performance. The aim of this work is to clarify how variations in base fluid ratio, nanoparticle loading, and magnetic field strength affect convective transport. The governing equations are solved numerically using the finite element method to capture coupled buoyancy and magnetohydrodynamic effects. The nanoparticle volume fractions are systematically varied from 0.1% to 0.5% to capture the impact of particle loading, while the Rayleigh number ranges from 10^3 to 10^6, and the Hartmann number from 0 to 40 , to assess the effects of buoyancy and magnetic fields. The results show that increasing the Rayleigh number significantly enhances convective heat transfer, while variations in base fluid composition lead to only marginal differences in the average Nusselt number. For example, the average Nusselt number increases by nearly one order of magnitude as Ra rises from 10^3 to 10^6, while nanoparticle addition yields up to $\sim 18\%$ enhancement, with copper providing the highest gains. In contrast, increasing Ha from 0 to 40 reduces the heat flux by as much as $\sim 22\%$. The inclusion of Cu and Al_2O_3 nanoparticles improves thermal performance, with copper demonstrating a greater enhancement due to its superior thermal conductivity. Furthermore, increasing the Hartmann number suppresses convective currents and reduces the total heat flux, especially near regions of high thermal activity. The wavy geometry intensifies convective mixing and promotes localized heat transfer, with observable peaks in the heat flux distribution aligned with the undulations of the hot wall. These findings highlight the synergistic effects of nanoparticle composition, base fluid selection, magnetic field control, and enclosure geometry on thermal transport, providing valuable insights for designing advanced cooling systems in electronics, energy, and thermal management applications. These insights highlight the relevance of the results for designing advanced cooling systems in electronics, renewable energy devices, and thermal management technologies.

2020 Mathematics Subject Classifications: 76N10

Key Words and Phrases: Hybrid nanofluid, water-ethylene glycol mixture, wavy enclosure

*Corresponding author.
DOI: https://doi.org/10.29020/nybg.ejpam.v18i4.6869

Email addresses: KKalbani@su.edu.om (K. Al Kalbani), Nanakira@su.edu.om (N. Anakira), AJassar@su.edu.om (A. Al Jassar), AAmourah@su.edu.om (A. Amourah), t_sasa@asu.edu.jo (T. Sasa)

Introduction

The pursuit of enhanced heat transfer efficiency is a critical endeavor in thermal engineering, propelled by the need for compact, energy-efficient systems in applications such as power generation, automotive cooling, solar thermal collectors, and electronic thermal management. Convective heat transfer, a key process in these systems, is often limited by the thermophysical properties of conventional fluids, such as water, ethylene glycol (EG), or their mixtures. To overcome these constraints, nanofluids-base fluids infused with nanoparticles-have emerged as a groundbreaking approach, offering a 28% increase in heat transfer coefficient with $Cu - TiO_2$ hybrid nanofluids in a $50 : 50$ water-EG mixture. This approach provides superior thermal conductivity and convective performance.

Hybrid nanofluids-fluids containing multiple nanoparticle types-have gained considerable attention due to their ability to synergistically enhance thermal properties beyond those of single-component nanofluids. Copper nanoparticles are renowned for their high thermal conductivity, while Al_2O_3 nanoparticles provide stability and affordability, making the Cu Al_2O_3 hybrid an attractive option for practical applications. The water-EG base fluid, widely employed in heat exchangers and cold-climate systems, exhibits adjustable properties-such as viscosity, density, and thermal conductivity-based on its composition. Recent studies have highlighted the promise of hybrid nanofluids in enhancing thermal performance. For example, Yaser et al. [1] reported a mixture, while Sidik et al. [2] observed that the thermal characteristics of the hybrid nanofluid were higher compared to the base fluid and the fluid containing single nanoparticles, respectively. However, most prior works have focused either on straight channels, simple cavities, or single-fluid nanofluids, with relatively fewer investigations addressing hybrid nanofluids in enclosures under combined buoyancy and magnetic field effects. In particular, systematic studies on the role of water-EG ratio in hybrid nanofluid-based wavy geometries remain scarce.

The wavy enclosure introduces a distinctive flow domain where natural convection is influenced by factors such as the Rayleigh number, nanoparticle volume fraction, and wall waviness (amplitude and wavelength). This geometry enhances heat transfer by increasing surface area and inducing flow perturbations that promote mixing. Bhardwaj et al. [3] found that wavy cavities can improve heat transfer compared to flat enclosures, while Al Kalbani and Uddin [4] noted an increase in the total heat flux at the heated wall by increasing the ripple parameter N. This research harnesses these geometric benefits, pairing them with the $Cu - Al_2O_3$ hybrid nanofluid in the specified water-EG ratios to optimize thermal performance. The motivation stems from the demand for efficient, versatile thermal systems that can operate across a range of conditions, from low-temperature refrigeration to high-temperature industrial processes.

Recent literature provides a strong foundation for this investigation. Tokgoz et al. [5] explore heat transfer enhancement in turbulent channel flow using corrugated ducts and alumina-water nanofluids. Results show that corrugation increases turbulence and heat transfer, and the nanofluid further improves thermal performance compared to pure water. Similarly, Said et al. [6] examine the thermophysical properties of nanodiamond

$+Fe_3O_4$ hybrid nanofluids (in water and water-EG mixtures) using experiments and predictive models, including MLR and MLRI. They found that the MLRI (R = 0.9996), MLR (R = 0.99989), MLR (R = 0.9999998), and MLRI (R = 0.9857) models demonstrated excellent predictive accuracy, with correlation coefficients indicating strong agreement between predicted and experimental values. Studies on wavy enclosures, such as those by Abdulkadhim et al. [7] and Cheng, C. Y.[8], emphasize geometry's role in amplifying buoyancy-driven convection. Despite these contributions, a direct connection between hybrid nanofluid composition (e.g., $Cu - Al_2O_3$ with variable water-EG ratios), magnetic field strength, and wavy enclosure design has not been comprehensively established in the literature. Further relevant research has been reported in [9–29].

This research employs a methodical approach to assess heat transfer enhancement by testing the $Cu - Al_2O_3$ hybrid nanofluid across the specified water-EG ratios: $95\% - 5\%, 90\% - 10\%, 80\% - 20\%, 60\% - 40\%$, and $50\% - 50\%$, as well as pure water and pure EG. Key variables include nanoparticle volume fractions (e.g., 0.1% to 0.5%), base fluid composition, and operating conditions (e.g., temperature gradients driving natural convection). The wavy enclosure is designed to maximize convective effects, and the study utilizes advanced experimental and/or numerical techniques to capture fluid flow and thermal behavior. Specifically, this work aims to investigate the heat transfer enhancement for pure water, pure ethylene glycol (EG), and various mixture ratios while also examining the effect of the wavy wall on flow patterns and streamlines. The objectives are to measure the enhancement in convective heat transfer (e.g., via Nusselt number) across these conditions and to analyze how the wavy geometry influences flow dynamics, providing insights into the interplay between fluid composition, nanoparticle effects, and enclosure design for next-generation thermal management strategies. In summary, the novelty of this study lies in combining $Cu - Al_2O_3$ hybrid nanofluids with variable water - EG ratios inside a wavywalled enclosure under magnetic field effects an area where literature remains limited. This work fills the gap by quantifying the coupled influence of nanoparticle loading, base fluid composition, and wall geometry on natural convection, offering new guidelines for designing efficient thermal management systems.

Physical Modelling

In the current study, we used nanofluidic flow to analyze time-independent, incompressible, laminar, and two-dimensional flow. The hydromagnetic and opposing gravitational forces were used to build a nano-fluidic model, where the equation space is a square of length L and filled with a $Cu - Al_2O_3$ /water - EG two-component hybrid nanofluid. The y-axis is normally next to the left wall, and the x-axis measures along the bottom surface in dimensional coordinates. The equations for wavy walls are:

$$x_{\text{left}} = 0.05\cos\left(\frac{N\pi y}{L}\right), \quad x_{\text{right}} = 0.05\cos\left(\frac{N\pi y}{L}\right) + L, \quad ; N = 4 \tag{1}$$

Regarding the coordinate system, a magnetic field with a strength of B_0 is applied. The upper and underside walls are insulated, and the right and left side walls are used to

isothermally cool and heat nanofluids at uniform temperatures of T_C and T_H correspondingly. It is always maintained that, $T_H > T_C$. The $Cu - Al_2O_3$ Hybrid nanoparticles and a water-ethylene glycol mixture were used as the base fluid in the current study. Fig. 1 illustrates the geometry and coordinate system schematically.

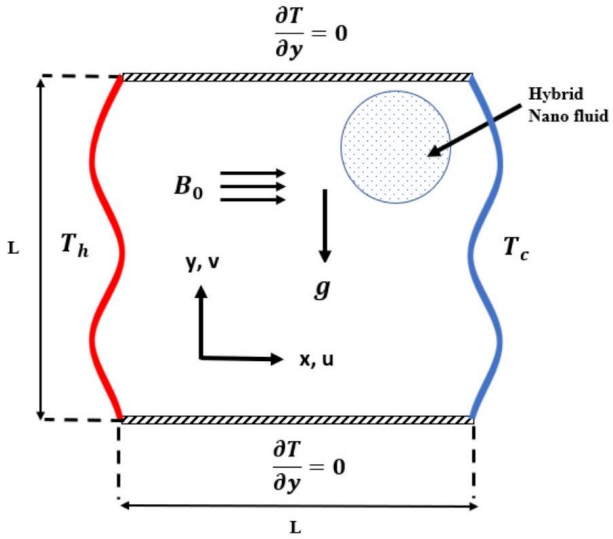

Fig. 1. Physical model's schematic view.

It is also expected that the reference solution and the nanomaterials are in thermodynamic equilibrium and that there is no slippage between the two media.

Table 1. Thermo-physical characteristics of solid nanoparticles (Oztop and Abu-Nada [30]) and the base fluid (pure water, pure EG, and mixtures of water–EG) as reported in [30], (Peyghambarzadeh et al. [31]), and (Bargal et al. [32]).

Items	c_p	ρ	k	μ	α	β	**Prandtl number**
Unit	$J/(kg\,K)$	kg/m^3	$W/(m\,K)$	$N\,s/m^2$	m^2/s	$1/K$	–
Pure water	4174	992	0.633	6.5×10^{-4}	1.5×10^{-7}	2.1×10^{-4}	4.286
Pure EG	2382	1101	0.256	9.5×10^{-3}	9.8×10^{-8}	5.7×10^{-4}	88.395
Water–EG (95%–5%)	4157	995	0.615	1.01×10^{-3}	1.49×10^{-7}	3.8×10^{-4}	6.827
Water–EG (90%–10%)	4090	1002	0.600	1.65×10^{-3}	1.46×10^{-7}	3.95×10^{-4}	11.248
Water–EG (80%–20%)	4020	1008	0.580	1.9×10^{-3}	1.43×10^{-7}	4.2×10^{-4}	13.169
Water–EG (60%–40%)	3500	1050	0.380	3×10^{-3}	1.03×10^{-7}	1.25×10^{-3}	27.632
Water–EG (50%–50%)	3340	1062	0.360	3.9×10^{-3}	1.015×10^{-7}	1.32×10^{-3}	36.183
Cu	385	8933	401	–	1.17×10^{-4}	1.67×10^{-5}	–
Al_2O_3	765	3970	40	–	1.32×10^{-5}	0.85×10^{-5}	–

Despite the density change in the body force element of the momentum equation estimated using the Boussinesq assumption, the physical properties of the nanofluids were assumed to be static. The acceleration due to gravity has a negative y-direction. Since all fixed boundaries are assumed to be rigid, the walls do not move. Table 1 is a listing of the thermophysical properties of nanofluids.

Mathematical Modelling

Assuming that the flow is continuous and laminar and that the nanofluid is Newtonian, a set of basic equations for nanofluids has been modified. The incompressible Navier-Stokes equations are used to model two-dimensional flow. The variation in density is analyzed using the Boussinesq approximation. Conservation of mass, momentum, and energy is addressed through the relevant mathematical equations. Given the above premises, the governing equations [33]for this model are presented as follows:

$$\frac{\partial u}{\partial x}+\frac{\partial v}{\partial y}=0 \tag{2}$$

$$u\frac{\partial u}{\partial x}+v\frac{\partial u}{\partial y}=-\frac{1}{\rho_{hnf}}\frac{\partial p}{\partial x}+\frac{\mu_{hnf}}{\rho_{hnf}}\left(\frac{\partial^2 u}{\partial x^2}+\frac{\partial^2 u}{\partial y^2}\right) \tag{3}$$

$$u\frac{\partial v}{\partial x}+v\frac{\partial v}{\partial y}=-\frac{1}{\rho_{hnf}}\frac{\partial p}{\partial y}+\frac{\mu_{hnf}}{\rho_{hnf}}\left(\frac{\partial^2 v}{\partial x^2}+\frac{\partial^2 v}{\partial y^2}\right)+g\left(T-T_C\right)\frac{(\rho\beta)_{hnf}}{\rho_{hnf}} \tag{4}$$

$$u\frac{\partial T}{\partial x}+v\frac{\partial T}{\partial y}=\alpha_{hnf}\left(\frac{\partial^2 T}{\partial x^2}+\frac{\partial^2 T}{\partial y^2}\right) \tag{5}$$

The parameters of the hybrid nanofluid are defined as follows ([33],[34]):

$$\rho_{hnf}=\rho_{bf}\left(1-\varphi_{hnf}\right)+\rho_{n1}\varphi_{n1}+\rho_{n2}\varphi_{n2} \tag{6}$$

$$(\rho\beta)_{hnf}=(\rho\beta)_{bf}\left(1-\varphi_{hnf}\right)+(\rho\beta)_{n1}\varphi_{n1}+(\rho\beta)_{n2}\varphi_{n2} \tag{7}$$

Where $\varphi_{hnf}=\varphi_{n1}+\varphi_{n2}$

$$\alpha_{hnf}=\frac{k_{hnf}}{(\rho c_p)_{hnf}}, \tag{8}$$

$$(\rho c_p)_{hnf}=\left(1-\varphi_{n1}-\varphi_{n2}\right)(\rho c_p)_{bf}+\varphi_{n1}\left(\rho c_p\right)_{n1}+\varphi_{n2}\left(\rho c_p\right)_{n2} \tag{9}$$

$$\mu_{hnf}=\frac{\mu_{bf}}{\left(1-\varphi_{n1}\right)^{2.5}\left(1-\varphi_{n2}\right)^{2.5}} \tag{10}$$

$$k_{hnf}=\frac{k_{n2}+2k_{nf}-2\varphi_{n2}\left(k_{nf}-k_{n2}\right)}{k_{n2}+2k_{nf}+\varphi_{n2}\left(k_{nf}-k_{n2}\right)}\left(k_{nf}\right) \tag{11}$$

$$k_{nf}=\frac{k_{n1}+2k_{bf}-2\varphi_{n1}\left(k_{bf}-k_{n1}\right)}{k_{n1}+2k_{bf}+\varphi_{n1}\left(k_{bf}-k_{n1}\right)}\left(k_{bf}\right) \tag{12}$$

The following are the different types of boundary conditions for the current investigation:

$$\begin{aligned} &u = v = 0, \quad T = T_H \quad \text{for } x_{\text{left}},\ 0 \le y \le L, && (a)\\ &u = v = 0, \quad T = T_C \quad \text{for } x_{\text{right}},\ 0 \le y \le L, && (b)\\ &u = v = 0, \quad \frac{\partial T}{\partial y} = 0 \quad \text{for } y = 0, L,\ 0 \le x \le L. && (c) \end{aligned} \tag{13}$$

The following transformations can be used to make the aforementioned equations dimensionless:

$$X = \frac{x}{L}, Y = \frac{y}{L}, U = \frac{uL}{\alpha_{bf}}, V = \frac{vL}{\alpha_{bf}}, P = \frac{pL^2}{\rho_{bf}\alpha^2{}_{bf}}, \quad \theta = \frac{T - T_C}{T_H - T_C} \tag{14}$$

With equation (14), the governing equations (2) through (5) can be expressed in the dimensionless form as follows:

$$\frac{\partial U}{\partial X} + \frac{\partial V}{\partial Y} = 0 \tag{15}$$

$$\left(\frac{\rho_{hnf}}{\rho_{bf}}\right)\left(U\frac{\partial U}{\partial X} + V\frac{\partial U}{\partial Y}\right) = -\frac{\partial P}{\partial X} + \frac{Pr}{(1-\varphi_{n1})^{2.5}(1-\varphi_{n2})^{2.5}}\left(\frac{\partial^2 U}{\partial X^2} + \frac{\partial^2 U}{\partial Y^2}\right),$$

$$\left(\frac{\rho_{hnf}}{\rho_{bf}}\right)\left(U\frac{\partial V}{\partial X} + V\frac{\partial V}{\partial Y}\right) \tag{16}$$

$$= -\frac{\partial P}{\partial Y} + \frac{Pr}{(1-\varphi_{n1})^{2.5}(1-\varphi_{n2})^{2.5}}\left(\frac{\partial^2 V}{\partial X^2} + \frac{\partial^2 V}{\partial Y^2}\right) + (Ra)(Pr)\frac{(\rho\beta)_{hnf}}{\rho_{bf}\beta_{bf}}\theta$$

$$-Ha^2\,\mathrm{Pr}\,V \tag{17}$$

$$U\frac{\partial \theta}{\partial X} + V\frac{\partial \theta}{\partial Y} = \frac{\alpha_{hnf}}{\alpha_{bf}}\left(\frac{\partial^2 \theta}{\partial X^2} + \frac{\partial^2 \theta}{\partial Y^2}\right) \tag{18}$$

Where $\mathrm{Pr} = \frac{\nu_{bf}}{\alpha_{bf}}$ is the Prandtl number, $Ra = \frac{g\beta_{bf}(T_H - T_C)L^3}{\alpha_{bf}\nu_{bf}}$ is the Rayleigh number and $Ha = B_0 L\sqrt{\frac{\sigma_{bf}}{\mu_{bf}}}$ is the Hartmann number.

The boundary conditions' dimensionless forms include:

$$\begin{aligned} &U = V = 0, \quad \theta = 1 \quad \text{for } X_{\text{left}},\ 0 \le Y \le 1, && (a)\\ &U = V = 0, \quad \theta = 0 \quad \text{for } X_{\text{right}},\ 0 \le Y \le 1, && (b)\\ &U = V = 0, \quad \frac{\partial \theta}{\partial Y} = 0 \quad \text{for } Y = 0, 1,\ 0 \le X \le 1. && (c) \end{aligned} \tag{19}$$

At the heated bottom wall, it is estimated that the local Nusselt number is:

$$Nu_{hnf} = -\left(\frac{k_{hnf}}{k_{bf}}\right)\left(\frac{\partial \theta}{\partial X}\right)_{X=0} \tag{20}$$

Furthermore, the local Nusselt number is integrated to produce the average Nusselt number:

$$\overline{Nu_{hnf}} = \int_0^1 Nu_{hnf} dY \tag{21}$$

Numerical Solution and Validation

Various mesh combinations of the geometry were tested to determine the optimal heat transfer rate and flow fields. During the grid test, a mixture of water and EG ($90\% - 10\%$) was selected as the base fluid for the experiment. The following parameter set combinations were used: $Ra = 10^5$, $\varphi_{n1} = 0.02, \varphi_{n2} = 0.02, \mathrm{Ha} = 20, \mathrm{Pr} = 11.25$, and $N = 4$. Four different non-standard grid systems were utilized in the simulation system to assess the expected number of elements for the constrained area. The arithmetic pattern is completed to be extremely accurately input in the typical Nusselt number (Nu_{av}) for the elements mentioned above, as shown in Table 2, in order to understand the mesh size. We noticed that the average Nusselt number (Nu_{av}) for 5554 elements showed a slight difference, in contrast to the results for the 7990 elements. Therefore, the grid sizes of 5554 and 7990 elements can be obtained to get accurate results, and 7990 triangle elements were considered in the simulation to generate the results.

Table 2. Grid sensitivity test at $Ra = 10^5$, $\varphi_{n1} = 0.02$, $\varphi_{n2} = 0.02$, Pr = 11.25, $Ha = 20$ and $N = 4$ for Cu-(Al_2O_3)/water(90%)-EG(10%) nanofluid at the left wavy wall of the cavity.

Elements	**3440**	**5554**	**7990**	**18120**
$\mathbf{Nu_{av}}$	3.023	3.005	3.002	2.989

We compared our results for the predetermined conditions with previously published results by Ghasemi et al. [35]. For this comparison, we selected: $\varphi_{n1} = 0, \varphi_{n2} = 0, 0.02, 0.06, N = 0$ for calculating the average Nusselt number presented in Table 3. In both studies, the average Nusselt number is calculated at the heated cavity wall for similar buoyancy forces. The current simulation results and the results of Ghasemi et al. [35] agree very closely. The numerical results of the study are now more credible and have been further validated.

Table 3. Comparison between the data of Ghasemi et al. [35] and the present work

Ra	$\boldsymbol{\varphi = 0}$		$\boldsymbol{\varphi = 0.02}$		$\boldsymbol{\varphi = 0.06}$	
	Present	Ghasemi et al. [35]	Present	Ghasemi et al. [35]	Present	Ghasemi et al. [35]
$\mathbf{10^3}$	1.002	1.001	1.060	1.160	1.184	1.184
10^4	1.181	1.179	1.224	1.302	1.319	1.291
10^5	3.137	3.151	3.180	3.138	3.259	3.108
10^6	7.82	7.907	7.965	7.979	8.230	8.098

1. Results and Discussion

To investigate the thermal and flow behavior of hybrid nanofluids in a wavy enclosure, a series of numerical simulations was conducted under various physical parameters. Isotherm distributions were analyzed for Rayleigh numbers ranging from 10^4 to 10^6, considering different base fluid compositions of water and ethylene glycol: $50\% - 50\%, 60\% - 40\%, 80\% - 20\%, 90\% - 10\%$, and $95\% - 5\%$. The mixture with equal proportions ($50\% - 50\%$) was adopted as the reference base fluid for comparative analysis.

Subsequent results show the total heat flux magnitude along the heated wall for different Rayleigh numbers and nanoparticle concentrations. Copper and aluminum oxide nanoparticles were introduced in different volume fractions to evaluate their respective influences on heat transfer characteristics.
Moreover, the effect of an externally applied magnetic field on flow structure and heat transfer was examined. The average Nusselt number was computed for each base fluid composition across a range of Rayleigh numbers and subsequently evaluated for varying concentrations of one type of nanoparticle while keeping the other type constant. These comprehensive simulations aim to elucidate the interplay between thermal buoyancy, magnetic forces, and nanoparticle-enhanced conductivity in complex enclosures.

Fig. 2 depicts the streamlines within the wavy enclosure for different Rayleigh numbers ($Ra = 10^4$, 10^5, 10^6) and varying water–ethylene glycol compositions, while keeping the nanoparticle volume fractions constant ($\phi_{n1} = 0.02$ for Cu, $\phi_{n2} = 0.02$ for Al_2O_3) and maintaining a fixed Hartmann number ($Ha = 20$).

For $Ra = 10^4$, the streamlines are concentrated along all four walls, with a higher density near the right and left vertical walls, indicating the dominance of conduction with weak convection. A single clockwise rotating cell forms at the cavity center as buoyancy forces begin to overcome viscous resistance, establishing a stable and symmetric circulation pattern. When Ra increases to 10^5, the buoyancy effect becomes stronger relative to viscous and magnetic damping forces, leading to thinner thermal and velocity boundary layers and an increase in streamline density along the vertical walls. The central vortex elongates diagonally, reflecting enhanced convective transport and stronger coupling between the upward and downward streams adjacent to the hot and cold walls. As Ra reaches 10^6, the flow becomes highly convective, with two secondary vortices developing near the upper-right and lower-left corners, and irregular motion appearing in the central region. This behavior signifies the transition toward a multi-cellular and partially unstable regime, where buoyancy-driven inertia starts to dominate despite the magnetic damping.

Furthermore, varying the water–EG mixing ratio did not noticeably alter the streamline topology, implying that the overall flow structure is primarily governed by buoyancy and magnetic effects rather than by modest variations in fluid thermophysical properties. The Rayleigh number dictates the strength and pattern of convection, while the Hartmann number ($Ha = 20$) acts to moderate the flow intensity without changing the fundamental circulation structure.

Fig. 3 illustrates the temperature contours (isotherms) within the wavy enclosure for various Rayleigh numbers ($Ra = 10^4$, 10^5, 10^6) and different compositions of the water–ethylene glycol base fluid, while maintaining constant nanoparticle volume fractions ($\phi_{n1} = 0.02$ for Cu, $\phi_{n2} = 0.02$ for Al_2O_3) and a fixed Hartmann number ($Ha = 20$).

As the Rayleigh number increases, the isotherms transition from a nearly vertical alignment to a more horizontal orientation. This transformation reflects the shift from conduction-dominated heat transfer at lower Ra to convection-dominated regimes at higher Ra. In low Rayleigh number cases, thermal diffusion governs the transport mechanism, resulting in stratified temperature fields. However, at higher Ra, buoyancy forces become more significant, inducing stronger convective currents that distort the temperature field and enhance thermal mixing.

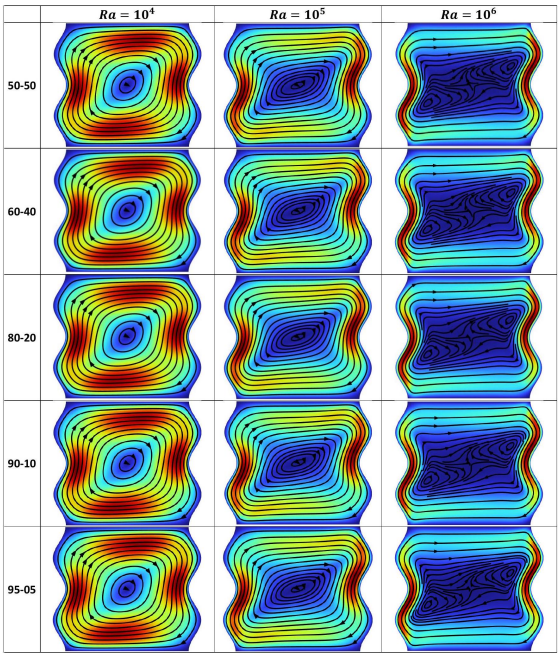

Fig 2. Streamlines for different Rayleigh numbers (Ra) and different percentages of water-ethylene glycol mixture when $\varphi_{n1} = 0.02$, $\varphi_{n2} = 0.02$, Ha = 20.

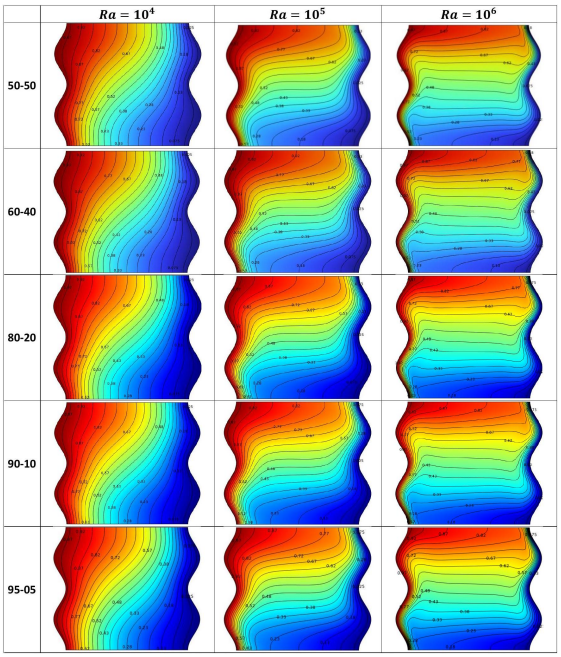

Fig 3. Isotherms for different Rayleigh numbers (Ra) and different percentages of water-ethylene glycol mixture when $\varphi_{n1} = 0.02$, $\varphi_{n2} = 0.02$, Ha $= 20$.

Additionally, the condensation of isotherms near the hot wall becomes more pronounced with increasing Ra, indicating intensified thermal gradients and localized heat transfer enhancement due to stronger convective activity adjacent to the heated boundary.

Across all configurations, elevated temperatures are observed near the hot wall and the upper region of the cavity. This is attributed to the upward movement of the heated fluid due to buoyancy, which accumulates along the top surface, especially under stronger convection.

Variations in the water-ethylene glycol mixture ratios result in only minor changes in the overall temperature distribution. This limited sensitivity is likely due to the relatively small difference in thermophysical properties (such as thermal conductivity and viscosity) between the considered mixtures, which exert only a secondary influence compared to the dominant effects of Rayleigh number and nanoparticle loading.

Fig. 4 presents the distribution of total heat flux magnitude along the heated wavy wall for various Rayleigh numbers, with fixed nanoparticle volume fractions of $\varphi_{n1} = 0.02$ (Cu) and $\varphi_{n2} = 0.02$ (Al_2O_3). The analysis is conducted for multiple water–ethylene glycol base fluid compositions, all of which exhibit qualitatively similar trends.

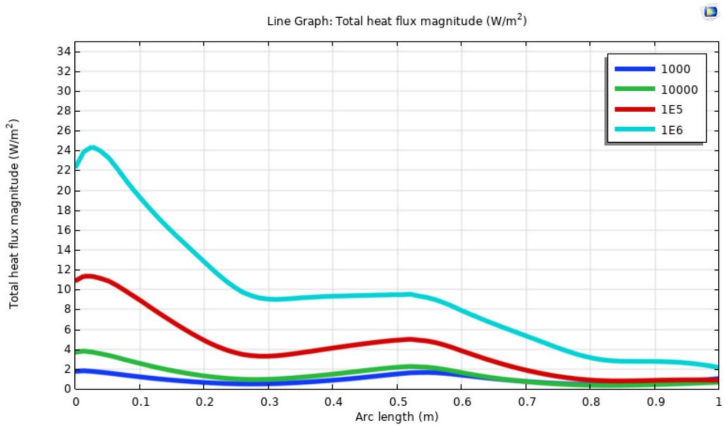

Fig. 4. Total heat flux magnitude for Rayleigh number (Ra) when $\varphi_{n1} = 0.02$, $\varphi_{n2} = 0.02$, Pr = 36.183, Ha = 20 (Cu–Al_2O_3/water(50%)–EG(50%)).

At a low Rayleigh number ($Ra = 10^3$), the heat flux profile remains nearly uniform with slight undulations that mirror the geometrical variations of the wavy boundary. This behavior is characteristic of conduction-dominated regimes, where heat transfer is primarily governed by temperature gradients and is not significantly influenced by fluid motion. The minor fluctuations in flux are attributed to the increased local surface area introduced by the wall corrugation.

As the Rayleigh number increases, the total heat flux along the heated wall exhibits a notable rise, especially toward the lower sections of the wall. This enhancement corresponds to the transition from conduction to convection-dominated heat transfer. In higher Ra regimes, buoyancy-driven flow enhances thermal transport by actively carrying heated fluid away from the hot wall and replacing it with cooler fluid. The bottom portion of the wavy wall experiences greater convective interaction due to the upward circulation of thermal plumes originating from that region, resulting in a localized increase in the magnitude of heat flux.

Despite varying the water-ethylene glycol mixing ratios, the overall distribution patterns remain consistent. This suggests that the influence of the Rayleigh number and nanoparticle loading on thermal convection outweighs the relatively modest variations in the base fluid's thermophysical properties. Nonetheless, fluids with higher water content, having lower viscosity and higher thermal conductivity, may support slightly more vigorous convection, further contributing to enhanced heat transfer.

Fig. 5 displays the distribution of total heat flux magnitude along the heated wavy wall for varying volume fractions of aluminum oxide nanoparticles (ϕ_{n2} ranging from 0 to 0.05) while maintaining a constant volume fraction of copper nanoparticles ($\phi_{n1} = 0.02$). The analysis is conducted under fixed thermal and flow conditions to isolate the effect of ϕ_{n2} on local heat transfer performance.

The resulting heat flux profiles exhibit a characteristic wavy pattern with two pronounced peaks: one located just above the lower segment of the wall and another near the mid-height of the wall. These peaks correspond to zones of intensified convective activity

driven by the local geometry and flow recirculation patterns within the enclosure. The distribution curves for different ϕ_{n2} values largely overlap along the wall, indicating minimal variation in overall flux except near the peak regions.

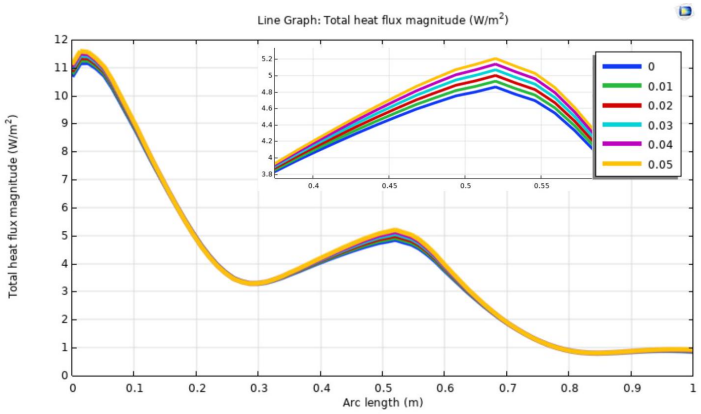

Fig. 5. Total heat flux magnitude for different values of φ_{n2} when $\varphi_{n1} = 0.02$, $Ra = 10^5$, $\mathrm{Pr} = 36.183$, $\mathrm{Ha} = 20$ (Cu–Al_2O_3/water(50%)–EG(50%)).

At these peak locations, a clear enhancement in the total heat flux magnitude is observed with increasing φ_{n2}, highlighting the role of aluminum oxide nanoparticles in boosting local thermal conductivity and, consequently, the rate of energy transfer to the fluid. This enhancement is attributed thermophysically to the higher effective thermal conductivity of the hybrid nanofluid, which increases as the concentration of Al_2O_3 rises. Although aluminum oxide has a lower thermal conductivity than copper, its synergistic interaction with Cu nanoparticles and the base fluid contributes positively to the overall heat transfer, especially in regions with steep temperature gradients.

A similar trend is observed when the role of φ_{n1} and φ_{n2} are interchanged-i.e., keeping φ_{n2} fixed and varying φ_{n1}. The corresponding results demonstrate analogous peak enhancement behavior with minor differences in magnitude and position, which will be discussed in detail in a subsequent section.

Fig. 6 presents the variation of total heat flux magnitude along the heated wavy wall for different Hartmann numbers (Ha = 0, 10, 20, 30, 40), illustrating the influence of magnetic field strength on heat transfer performance in the presence of electrically conducting hybrid nanofluids.

Across all cases, the heat flux profiles exhibit a characteristic wavy decreasing pattern, with two distinct local maxima—one located near the lower section and the other near the mid-height of the wall. These peak regions correspond to zones of enhanced convective motion and intensified thermal gradients induced by the enclosure's wavy geometry.

As the Hartmann number increases, a systematic reduction in the total heat flux magnitude is observed. This attenuation in heat transfer can be attributed to the magnetohydrodynamic (MHD) damping effect: the presence of a transverse magnetic field introduces Lorentz forces that act as a resistive force against fluid motion. These forces

suppress the buoyancy-driven convective currents that are responsible for enhancing heat transport, thereby shifting the dominant heat transfer mechanism toward conduction, especially at higher Ha values.

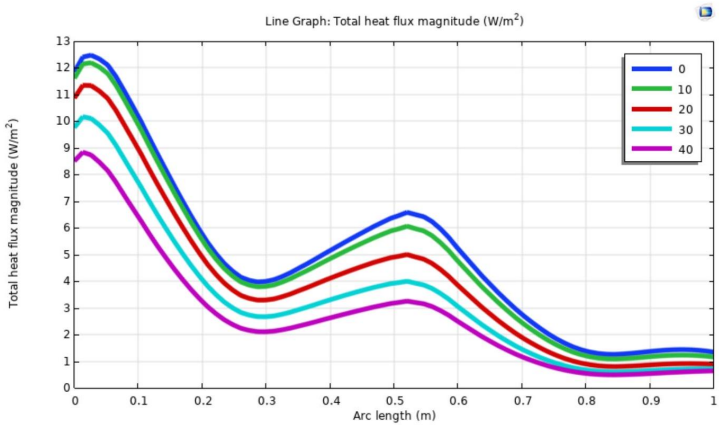

Fig. 6. Total heat flux magnitude for the Hartmann number (Ha) when $\varphi_{n1} = 0.02$, $\varphi_{n2} = 0.02$, Pr = 36.183, $Ra = 10^5$ (Cu–Al_2O_3/water(50%)–EG(50%)).

Notably, the divergence between the flux curves becomes more noticeable at the peak regions. This suggests that the localized convective enhancements, which are highly sensitive to fluid motion, are more significantly damped under stronger magnetic fields. In contrast, the regions between peaks, where conduction plays a relatively larger role, are less affected.

Overall, the results confirm that increasing magnetic field strength exerts a stabilizing and suppressive influence on convective transport, leading to reduced thermal efficiency along the heated wall. This highlights the critical interplay between electromagnetic control and thermal performance in MHD applications involving hybrid nanofluids.

Table 4 presents the average Nusselt number for various Rayleigh numbers ($Ra = 10^3$, 10^4, 10^5, 10^6) and different water–ethylene glycol base fluid compositions: 50%–50%, 60%–40%, 80%–20%, 90%–10%, and 95%–5%. The concentrations of copper and aluminum oxide nanoparticles are fixed at $\varphi_{n1} = 0.02$ and $\varphi_{n2} = 0.02$, respectively.

As expected, the average Nusselt number increases significantly with the rising Rayleigh number for all base fluid mixtures. This trend reflects the transition from conduction-dominated to convection-dominated heat transfer regimes. At low Ra, thermal energy is primarily transferred through molecular diffusion, resulting in lower Nusselt numbers. With increasing Ra, the buoyancy-driven flow becomes stronger, enhancing thermal transport via fluid motion and leading to a substantial increase in convective heat transfer rates.

In contrast, the variation in average Nusselt number among the different water–ethylene glycol mixtures is relatively small across all Rayleigh numbers. This limited sensitivity can be attributed to the moderate changes in thermophysical properties—such as thermal conductivity, viscosity, and specific heat—across the selected mixing ratios. Although increasing the water content generally improves thermal conductivity and reduces

	50 − 50	**60 − 40**	**80 − 20**	**90 − 10**	**95 − 05**
Ra $= 10^3$	0.963	0.963	0.963	0.964	0.964
Ra $= 10^4$	1.345	1.345	1.345	1.345	1.345
Ra $= 10^5$	3.719	3.720	3.721	3.722	3.722
Ra $= 10^6$	**8.584**	**8.593**	**8.595**	**8.597**	**8.602**

Table 4. Average Nusselt number for different percentages of Water–Ethylene Glycol base fluid when $\varphi_{n1} = 0.02$, $\varphi_{n2} = 0.02$, Ha $= 20$.

viscosity (thus promoting convection), the impact of these variations is overshadowed by the dominant influence of the Rayleigh number and the presence of thermally conductive nanoparticles.

These findings suggest that, within the examined range of base fluid compositions, the enhancement in heat transfer is governed more strongly by buoyancy effects and nanoparticle loading than by the specific ratio of water to ethylene glycol.

Fig. 7 illustrates the variation of the average Nusselt number with increasing nanoparticle volume fractions of copper ($\varphi_{n1} = 0$ to 0.05) and aluminum oxide ($\varphi_{n2} = 0$ to 0.05), under a fixed Rayleigh number of $Ra = 10^5$. In the first case (red curve), the volume fraction of Al_2O_3 is held constant at $\varphi_{n2} = 0.02$, while $\varphi_{n1}(Cu)$ varies. In the second case (blue curve), the volume fraction of Cu is fixed at $\varphi_{n1} = 0.02$, and $\varphi_{n2}\,(Al_2O_3)$ is varied.

Both trends exhibit a monotonic increase in the average Nusselt number with increasing nanoparticle volume fraction, confirming the positive effect of nanoparticle loading on convective heat transfer. However, the enhancement is more pronounced in the case of copper nanoparticles. For equivalent volume fractions, the red curve lies consistently above the blue curve, indicating that increasing φ_{n1}(Cu) results in greater thermal performance compared to increasing φ_{n2} (Al_2O_3).

This difference can be thermophysically explained by the superior thermal conductivity of copper relative to aluminum oxide. The inclusion of highly conductive Cu nanoparticles significantly boosts the effective thermal conductivity of the hybrid nanofluid, facilitating more efficient heat transport. Although Al_2O_3 contributes to thermal enhancement, its lower intrinsic conductivity yields a more modest improvement when added in the same proportions.

These results highlight the importance of nanoparticle selection in hybrid nanofluid formulations and underscore the dominant role of copper in enhancing convective heat transfer under moderate to high Rayleigh number conditions.

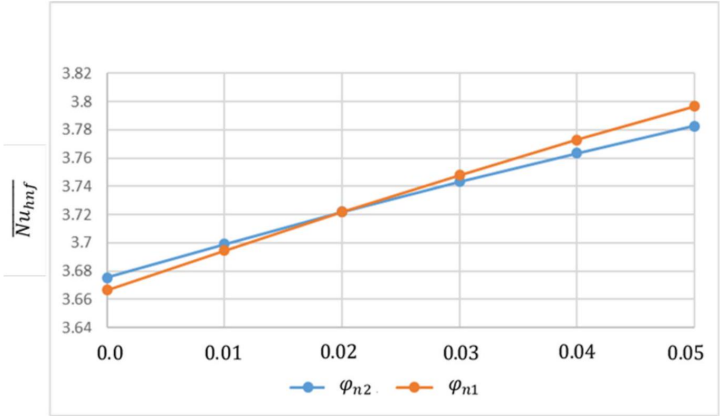

Fig. 7. Average Nusselt number for different values of φ_{n1} and φ_{n2} when Ha $= 20$, Pr $= 36.183$, $Ra = 10^5$ (Cu–Al_2O_3/water(50%)–EG(50%)).

Conclusion

A comprehensive numerical investigation was conducted to analyze the convective heat transfer characteristics of a hybrid nanofluid consisting of copper (Cu) and aluminum oxide (Al_2O_3) nanoparticles, which were dispersed in various mixtures of water and ethylene glycol as the base fluid. This analysis took place within a wavy-walled enclosure under the influence of magnetic fields. The simulations considered a wide range of Rayleigh numbers, nanoparticle volume fractions, and Hartmann numbers to evaluate the effects of thermal buoyancy, nanoparticle loading, base fluid composition, and magnetic field intensity on heat transfer performance.

The key findings can be summarized as follows:

- Rayleigh Number Influence: The transition from conduction-dominated to convectionenhanced regimes was clearly observed with increasing Rayleigh number, as reflected in both the isotherm patterns and the significant rise in the average Nusselt number.
- Base Fluid Composition: Variations in water-ethylene glycol ratios exhibited only minor influence on the thermal behavior, indicating that the base fluid's thermophysical properties play a secondary role compared to buoyancy forces and nanoparticle effects.
- Nanoparticle Volume Fraction: Both Cu and Al_2O_3 nanoparticles contributed to enhanced heat transfer. However, Cu demonstrated a more substantial effect, attributable to its higher thermal conductivity. Hybrid nanofluids with increasing Cu volume fraction achieved superior Nusselt numbers compared to those with increasing Al_2O_3 content under fixed Rayleigh conditions.
- Magnetic Field Effects: The application of a transverse magnetic field (modeled through varying Hartmann numbers) suppressed convective motion due to the

Lorentz force, resulting in decreased total heat flux along the heated wall. The dampening effect was especially pronounced in regions of high thermal activity.

Overall, the study confirms the potential of $Cu - Al_2O_3$ /water-ethylene glycol hybrid nanofluids to enhance thermal performance in thermally driven enclosures. These insights are particularly valuable for the development of advanced cooling technologies in applications such as electronic device thermal management, energy systems, and microfluidic heat exchangers, where precise thermal control is critical under variable operating conditions.

Directions for Future Research

While this study offers valuable numerical insights, it highlights the need for further multi-faceted research to advance the field. Experimental validation of the predicted thermal performance remains a critical priority to verify model accuracy under practical conditions. Future work should also explore a wider range of nanoparticle materials - including graphene-based composites - and non-spherical morphologies to optimize thermal conductivity without undue viscosity increases. Expanding simulations to three-dimensional and transient flows with realistic boundary conditions would greatly improve practical relevance. Additionally, thorough investigation into nanofluid stability, rheological behavior, and pumping power requirements is essential to assess overall energy efficiency. Finally, integrating multi-physics interactions such as electro hydrodynamic or thermoelectric effects could enable next-generation thermal management solutions for advanced microelectronics and microfluidic devices.

Acknowledegements

The authors gratefully acknowledge the financial support provided by the Ministry of Higher Education, Research and Innovation (MoHERI), Oman, through the Block Funding Program at Sohar University (SU Ref: SU/BFP/RG/2024/07). This support was essential for the successful completion of this research.

References

[1] Muhammad Yasir, Masood Khan, AS Alqahtani, and MY Malik. Heat generation/absorption effects in thermally radiative mixed convective flow of zn- tio2/h2o hybrid nanofluid. *Case Studies in Thermal Engineering*, 45:103000, 2023.

[2] Nor Azwadi Che Sidik, Isa Muhammad Adamu, Muhammad Mahmud Jamil, GHR Kefayati, Rizalman Mamat, and G Najafi. Recent progress on hybrid nanofluids in heat transfer applications: a comprehensive review. *International communications in heat and mass Transfer*, 78:68–79, 2016.

[3] Saurabh Bhardwaj, Amaresh Dalal, and Sukumar Pati. Influence of wavy wall and non-uniform heating on natural convection heat transfer and entropy generation inside porous complex enclosure. *Energy*, 79:467–481, 2015.

[4] Khamis Al Kalbani and MJ Uddin. Convective heat transfer of cu-al 2 o 3/water hybrid nanofluid flow in a cavity having vertical wavy sides. *Iraqi Journal of Science*, 66(2), 2025.

[5] Nehir Tokgoz, E Alıç, Ö Kaşka, and MM Aksoy. The numerical study of heat transfer enhancement using al2o3-water nanofluid in corrugated duct application. *journal of thermal engineering*, 4(3):1984–1997, 2018.

[6] Zafar Said, Mehdi Jamei, L Syam Sundar, AK Pandey, A Allouhi, and Changhe Li. Thermophysical properties of water, water and ethylene glycol mixture-based nanodiamond+ fe3o4 hybrid nanofluids: An experimental assessment and application of data-driven approaches. *Journal of Molecular Liquids*, 347:117944, 2022.

[7] Ammar Abdulkadhim, Hameed K Hamzah, Farooq Hassan Ali, Çağatay Yıldız, Azher M Abed, Esam M Abed, and Müslüm Arıcı. Effect of heat generation and heat absorption on natural convection of cu-water nanofluid in a wavy enclosure under magnetic field. *International Communications in Heat and Mass Transfer*, 120:105024, 2021.

[8] Ching-Yang Cheng. Natural convection heat and mass transfer near a vertical wavy surface with constant wall temperature and concentration in a porous medium. *International Communications in Heat and Mass Transfer*, 27(8):1143–1154, 2000.

[9] M. Hassan, M. Marin, R. Ellahi, and S. Z. Alamri. Exploration of convective heat transfer and flow characteristics synthesis by cu-ag/water hybrid-nanofluids. *Heat Transfer Research*, 49(18), 2018.

[10] D. Madhesh, R. Parameshwaran, and S. Kalaiselvam. Experimental investigation on convective heat transfer and rheological characteristics of cu-tio2 hybrid nanofluids. *Experimental Thermal and Fluid Science*, 52:104–115, 2014.

[11] M. N. Labib, M. J. Nine, H. Afrianto, H. Chung, and H. Jeong. Numerical investigation on the effect of base fluids and hybrid nanofluid in forced convective heat transfer. *International Journal of Thermal Sciences*, 71:163–171, 2013.

[12] N. A. C. Sidik, I. M. Adamu, M. M. Jamil, G. H. R. Kefayati, R. Mamat, and G. Najafi. Recent progress on hybrid nanofluids in heat transfer applications: a comprehensive review. *International Communications in Heat and Mass Transfer*, 78:68–79, 2016.

[13] G. P. Ashwinkumar, S. P. Samrat, and N. Sandeep. Convective heat transfer in mhd hybrid nanofluid flow over two different geometries. *International Communications in Heat and Mass Transfer*, 127:105563, 2021.

[14] K. G. Kumar, M. G. Reddy, A. Aldalbahi, M. Rahimi-Gorji, and M. Rahaman. Application of different hybrid nanofluids in convective heat transport of carreau fluid. *Chaos, Solitons & Fractals*, 141:110350, 2020.

[15] T. Tayebi and A. J. Chamkha. Magnetohydrodynamic natural convection heat transfer of hybrid nanofluid in a square enclosure in the presence of a wavy circular conductive cylinder. *Journal of Thermal Science and Engineering Applications*, 12(3):031009, 2020.

[16] S. Hussain, T. Tayebi, T. Armaghani, A. M. Rashad, and H. A. Nabwey. Conjugate natural convection of non-newtonian hybrid nanofluid in a wavy-shaped enclosure.

Applied Mathematics and Mechanics, 43(3):447–466, 2022.

[17] M. M. Ali, R. Akhter, and M. A. Alim. Hydromagnetic natural convection in a wavy-walled enclosure equipped with a hybrid nanofluid and heat-generating cylinder. *Alexandria Engineering Journal*, 60(6):5245–5264, 2021.

[18] S. Hansda and S. K. Pandit. Thermosolutal hydromagnetic mixed convective hybrid nanofluid flow in a wavy-walled enclosure. *Journal of Magnetism and Magnetic Materials*, 572:170580, 2023.

[19] A. Gaber, M. Mohamed, and G. Moatimid. Maxwell hybrid nanofluid (cu-al2o3/water) and (cuo-ag/water) near a stagnation point above an extending sheet. *European Journal of Pure and Applied Mathematics*, 18(1):5773–5773, 2025.

[20] A. S. Omer. Marangoni convection in hybrid nanofluid flow over a disk. *European Journal of Pure and Applied Mathematics*, 18(2):6206–6206, 2025.

[21] N. Biswas, D. K. Mandal, N. K. Manna, R. S. R. Gorla, and A. J. Chamkha. Magnetohydrodynamic thermal characteristics of water-based hybrid nanofluid-filled non-darcian porous wavy enclosure: effect of undulation. *International Journal of Numerical Methods for Heat & Fluid Flow*, 32(5):1742–1777, 2022.

[22] S. Munir and Y. U. U. B. Turabi. Impact of heated wavy wall and hybrid nanofluid on natural convection in a triangular enclosure with embedded cold cylinder under inclined magnetic field. *Arabian Journal for Science and Engineering*, 50(6):4007–4020, 2025.

[23] K. Hosseinzadeh, M. E. Moghaddam, S. Nateghi, M. B. Shafii, and D. D. Ganji. Radiation and convection heat transfer optimization with mhd analysis of a hybrid nanofluid within a wavy porous enclosure. *Journal of Magnetism and Magnetic Materials*, 566:170328, 2023.

[24] R. P. Sharma, B. K. Barik, V. V. Kumar, and A. Sharma. Illustration of low oscillating magnetic field on sodium alginate-based hybrid nanofluid flow between two revolving disks: An artificial neural network-based study. *Engineering Applications of Artificial Intelligence*, 155:111101, 2025.

[25] A. Sharma and R. P. Sharma. Utilizing neural networks to illustrate the dynamics of viscous fluid flow over curved surface with homogeneous and heterogeneous reactions. *Engineering Applications of Artificial Intelligence*, 159:111629, 2025.

[26] S. Praharaj and R. P. Sharma. Optimization of heat transfer characteristics in williamson fluid flow over a permeable riga surface for advanced engineering applications. *Multiscale and Multidisciplinary Modeling, Experiments and Design*, 8(7):324, 2024.

[27] V. V. Kumar and R. P. Sharma. Entropy generation minimization in nuclear reactor cooling via rough rotating disk: a statistical approach. *Multiscale and Multidisciplinary Modeling, Experiments and Design*, 8(5):245, 2025.

[28] S. Shukla, R. P. Sharma, R. J. Punith Gowda, and B. C. Prasannakumara. Elastic deformation effect on carboxymethyl cellulose water-based (tio2-ti6al4v) hybrid nanoliquid over a stretching sheet with an induced magnetic field. *Numerical Heat Transfer, Part A: Applications*, 84(11):1401–1415, 2023.

[29] R. P. Sharma and S. R. Mishra. Effect of higher order chemical reaction on mag-

netohydrodynamic micropolar fluid flow with internal heat source. *International Journal of Fluid Mechanics Research*, 47(2), 2020.

[30] H. F. Oztop and E. Abu-Nada. Numerical study of natural convection in partially heated rectangular enclosures filled with nanofluids. *International Journal of Heat and Fluid Flow*, 29(5):1326–1336, 2008.

[31] S. M. Peyghambarzadeh, S. H. Hashemabadi, S. M. Hoseini, and M. S. Jamnani. Experimental study of heat transfer enhancement using water/ethylene glycol-based nanofluids as a new coolant for car radiators. *International Communications in Heat and Mass Transfer*, 38(9):1283–1290, 2011.

[32] M. H. Bargal, A. N. Allam, M. E. Zayed, Y. Wang, and L. M. Alhems. Comprehensive parametric study and sensitivity analysis of automotive radiators using different water/ethylene glycol mixtures: Toward thermo-hydraulic performance and heat transfer characteristics optimization. *Heat Transfer*, 54(1):244–270, 2025.

[33] F. H. Lai and Y. T. Yang. Lattice boltzmann simulation of natural convection heat transfer of al2o3/water nanofluids in a square enclosure. *International Journal of Thermal Sciences*, 50(10):1930–1941, 2011.

[34] R. Nasrin and M. A. Alim. Free convective flow of nanofluid having two nanoparticles inside a complicated cavity. *International Journal of Heat and Mass Transfer*, 63:191–198, 2013.

[35] B. Ghasemi, S. M. Aminossadati, and A. Raisi. Magnetic field effect on natural convection in a nanofluid-filled square enclosure. *International Journal of Thermal Sciences*, 50(9):1748–1756, 2011.

Nomenclature

Dimensional quantities

A amplitude [m]
B_0 magnetic field strength [kg/s2. A]
c_p specific heat at constant pressure [J/kgK]
g gravitational acceleration [m/s2]
k thermal conductivity [W/mK]
L enclosure length [m]
N undulation parameter [m]
p dimensional fluid pressure [Pa]
T Temperature [K]
u, v dimensional velocity components [m/s]
x, y dimensional coordinates [m]
Dimensionless quantities
Ha Hartmann number [-]
Nu Nusselt number [-]
P dimensionless fluid pressure [-]
Pr Prandtl number [-]
Ra Rayleigh number [-]

U, V dimensionless velocity components [-]
X, Y dimensionless coordinates [-]

Greek symbols

α thermal diffusivity [m^2/s]
β thermal expansion coefficient [1/K]
θ dimensionless temperature [-]
μ dynamic viscosity [Ns/m^2]
v kinematic viscosity [m^2/s]
ρ density [kg/m^3]
σ electrical conductivity [S/m]
φ nanoparticle volume fraction [-]

Subscript

av average
bf base fluid
C cold wall
H hot wall
hnf hybrid nanofluid
$n1$ copper nanoparticle
$n2$ aluminum oxide nanoparticle
nf nanofluid